A complex multi-chamber magmatic system beneath a late Cenozoic volcanic field: evidence from CSDs and thermobarometry of clinopyroxene from a single nephelinite flow (Djbel Saghro, Morocco)

JULIEN BERGER[1,2,3], NASSER ENNIH[4], JEAN-PAUL LIÉGEOIS[1], COLLIN NKONO[2], JEAN-CLAUDE C. MERCIER[3] & DANIEL DEMAIFFE[2]

[1]*Section de Géologie Isotopique, Musée Royal de l'Afrique Centrale, 3080 Tervuren, Belgium (e-mail: julien.berger@africamuseum.be)*

[2]*Laboratoire de Géochimie Isotopique et Géodynamique Chimique, CP160/02, Université Libre de Bruxelles (ULB), 1050 Brussels, Belgium*

[3]*Centre Littoral de Géophysique, UMR-CNRS 6250 "LIENSs", Université de La Rochelle, 17402 La Rochelle Cedex-1, France*

[4]*Laboratoire de Géodynamique, Université d'El Jadida, BP20, 24000 El Jadida, Morocco*

Abstract: We used quantitative textural measurement, electron microprobe microanalysis and thermobarometry on clinopyroxene from a Cenozoic pyroxene-nephelinite flow located along the northern boundary of the West African craton to decipher magma differentiation processes in underlying magma chambers. The crystal size distributions of clinopyroxene phenocrysts show straight but also curved and kinked patterns and the clinopyroxene show large compositional variations in a single flow (Mg-number 48–88). These observations are strong evidence for magma mixing between a nephelinite magma and a more differentiated phonolitic melt at depth. Detailed thermobarometry on these clinopyroxene shows that at least three magma chambers are present below Saghro and that they are emplaced at the main physical interface within the lithosphere: (1) at the crust–mantle boundary, where the mantle-derived nephelinite has been mixed with a pre-existing phonolitic magma chamber; (2) at the lower–upper crust boundary; (3) close to the surface in a sub-volcanic magma chamber. Some high-pressure phenocrysts (up to 14 kbar) have also probably crystallized within the upper lithospheric mantle. The high clinopyroxene proportion in samples from the base of the flow is thought to reflect crystal settling during cooling of the nephelinite flow at the surface.

Lava flows at the surface are generally considered as simple, rather homogeneous geochemical systems. Nevertheless, complex crystallization histories before eruption can sometimes be recognized by the presence of complex zoning of phenocrysts, implying complex chemical evolution of the magma (fractional crystallization, assimilation, local disequilibrium) and/or changes in the physical conditions (pressure and temperature) during magma rise and solidification (Duda & Schmincke 1985; Dobosi 1989; Bachmann & Dungan 2002). Phenocryst resorption is also strong evidence of solid–liquid disequilibrium during magmatic evolution (O'Brien *et al.* 1988; Streck *et al.* 2002). Understanding the crystallization conditions of a magma before its eruption has many petrological consequences: the $P-T$ conditions have a direct effect on the composition of the fractionating phases and thus on the geochemical evolution trend of the volcanic series (Grove & Baker 1984; Scoates *et al.* 2006). The physical conditions that prevailed during the crystallization steps of the magma development are thus needed to model the magmatic evolution. In addition, the pressure of crystallization of the phenocrysts is directly linked to the depth of the magma chamber. A detailed thermobarometric approach to the phenocryst assemblage could then be used to infer the depth of the magma chambers beneath active or extinct volcanoes and, by extension, the depth of the main physical interfaces within the lithosphere (crust–mantle boundary, elastic–plastic intracrustal boundary, etc.).

We show in this paper that, by a combination of quantitative textural (crystal size distribution; CSD) and chemical (electron microprobe analysis; EMPA) studies on clinopyroxene phenocrysts coupled with thermobarometric investigations on a

From: ENNIH, N. & LIÉGEOIS, J.-P. (eds) *The Boundaries of the West African Craton.* Geological Society, London, Special Publications, **297**, 509–524.
DOI: 10.1144/SP297.25 0305-8719/08/$15.00

single Cenozoic nephelinite flow from the Djbel Saghro field (Morocco), the complete and complex evolution of the magma can be deciphered. We demonstrate that polybaric differentiation combined with magma mixing has a strong imprint on the compositional zoning of phenocrysts, and on the texture of the nephelinite rock itself. Also, late-stage cooling of the magma at the surface has an effect on the distribution of phenocrysts within the flow.

Geological setting

The Saghro volcanic field is located at the eastern edge of the Saghro inlier in the Anti-Atlas of Morocco (Fig. 1). The volcanic activity occurred in two periods during the Cenozoic (Berrahma *et al.* 1993): the Late Miocene phase (9.6–7.6 Ma) was concentrated in the south and the Late Pliocene (*c*. 2.9 Ma) in the north. The Saghro volcanic field is as large (*c*. 1500 km^2) as the contemporaneous huge Sirwa stratovolcano (25 km in diameter) located further to the west but in the Saghro inlier. All Cenozoic volcanic exposures (lava flows, necks and minor pyroclastic deposits) are of small extent.

The chemistry of the erupted lavas is typically bimodal, consisting of silica-undersaturated nephelinites and phonolites. A single exposure of intermediate lava with phono-tephrite composition is known (Ibhi 2000, and our unpublished data). The Saghro suite of lavas is peralkaline in overall composition and is associated with a carbonatitic magmatism expressed as carbonatite xenoliths in the nephelinites (Ibhi *et al.* 2002).

The geodynamical event responsible for the onset of this alkaline magmatism is still debated. Considering that the Saghro volcanic field, the Sirwa stratovolcano and the Canary Islands are located on the same structural line, some workers (Hoernle & Schmincke 1993) have related this volcanism to a mantle plume rising from the base of the upper mantle. In contrast, others (Liégeois *et al.* 2005), taking into account the fact that the Cenozoic alkaline magmatism of Morocco, and of West Africa as a whole, occurred along Pan-African or Variscan structures reactivated during the Alpine orogeny, have related the volcanism to the paroxysmal events of the Africa–Europe convergence. The Saghro and Sirwa volcanic fields are located along the northern boundary of the West African craton, just to the south of the current High Atlas mountain range.

We focused our investigations on a 12 m thick flow of pyroxene-nephelinite from Foum el Kous (Fig. 1). This lava flow rests upon a contemporary flow of olivine-nephelinite itself covering continental Cretaceous sediments. The eruption of the pyroxene-nephelinite flow has been dated at *c*. 2.9 Ma (whole-rock K–Ar, Berrahma *et al.* 1993).

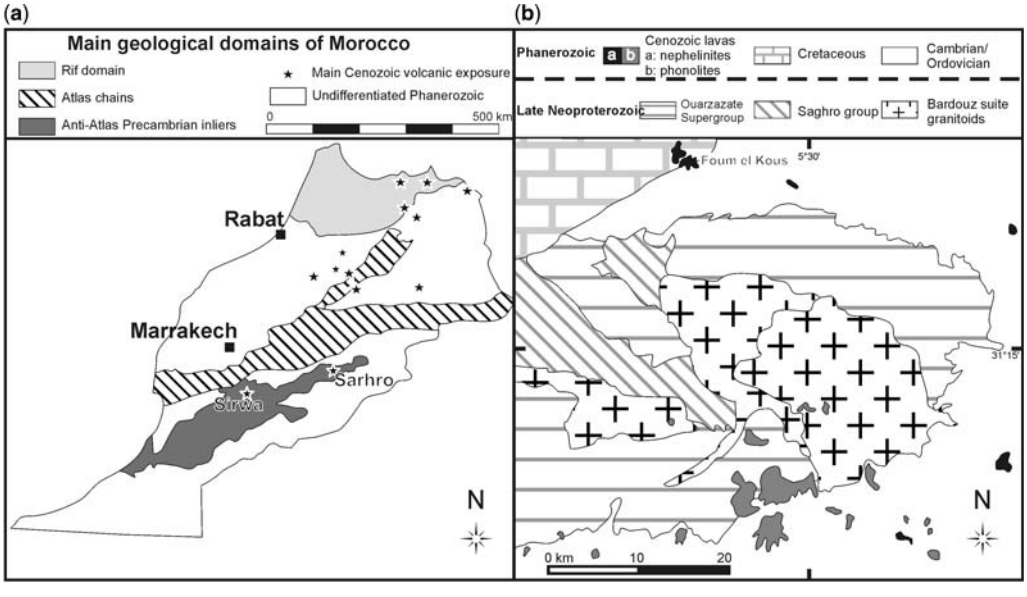

Fig. 1. (**a**) Location of the Saghro Cenozoic volcanic field within Morocco and (**b**) a simplified geological map of the eastern edge of the Saghro inlier (modified after Ibhi *et al.* 2002).

Sample description and whole-rock composition

Under the microscope the nephelinite lava flow consists of phenocrysts of Ti-augite, olivine and minor Ti-magnetite in a fine-grained groundmass dominated by clinopyroxene, nepheline and Ti-magnetite, with accessory apatite, biotite and perovskite. Olivine phenocrysts (<1 mm) are generally resorbed with corrosion gulfs and partial iddingsitization of their borders. The phenocrysts are unzoned with the notable exception of clinopyroxene, which displays complex zoning patterns. Four types of clinopyroxene have been recognized on a textural basis.

Type 1 clinopyroxenes are zoned euhedral crystals (>700 μm) with dark greenish brown cores surrounded by light brown mantles and thin dark brown rims (Fig. 2a and b). The central dark core is always anhedral to subhedral and exhibits complex zonations. It contains mineral (biotite, amphibole) and abundant fluid inclusions. Groundmass minerals (nepheline, Ti-magnetite and apatite) are present as inclusions at the contact zone between the dark core and the light mantle zone. The latter is unzoned, but in some samples it evolves gradually towards dark rim, which also contains numerous inclusions of the groundmass minerals.

Type 2 clinopyroxenes are small (<500 μm), euhedral, complexly zoned crystals with green cores (Fig. 2c and d). The complete succession of zones is: in the centre, an anhedral green core with numerous inclusions of the groundmass minerals, rimmed by an anhedral dark green part, itself surrounded by a light brown mantle, and finally a thin rim of brown clinopyroxene with numerous inclusions of nepheline, Ti-magnetite and apatite.

Type 3 clinopyroxenes are small (<500 μm) light brown phenocrysts with tabular shapes (Fig. 2e). They rarely exhibit sector zoning but have a distinct core and rim. In contrast to the core, which is free of inclusions, the dark brown augitic rim has numerous inclusions of the matrix minerals. The border of the crystals sometimes shows resorption features marked by corrosion gulfs filled with matrix minerals (clinopyroxene, nepheline, Ti-magnetite).

Type 4 clinopyroxenes (50 and 200 μm) are groundmass phases with granular or acicular habits. They are in textural equilibrium with the other matrix minerals and sometimes contain inclusions of Ti-magnetite, apatite, nepheline and perovskite.

One of the most striking features of this lava flow is the presence of numerous megacrysts. Amphibole and olivine have been observed (Ibhi 2000) but clinopyroxene is by far the most abundant. These clinopyroxene megacrysts are euhedral to subhedral, but occasionally only the relicts of larger broken crystals are preserved (Fig. 2f). They are fractured and rich in fluid inclusions but they are not zoned, nor do they have mineral inclusions, except for a thin rim of darker clinopyroxene containing inclusions of the groundmass minerals.

Xenoliths are abundant; they are generally rounded and do not exceed 5 cm. They are mainly monomineralic clinopyroxenite with accessory biotite, apatite and olivine, but subordinate mantle peridotites and carbonatites have been found (Ibhi *et al.* 2002). The xenoliths generally show equilibrated medium-grained granular texture. The clinopyroxene is zoned and has a dark core and a light brown rim. The clinopyroxene from the xenoliths contains numerous small vitreous inclusions that probably formed during the strong temperature increase undergone by the pyroxenites during their ascent in the host lava.

The whole-rock composition of the flow is rather homogeneous (Fig. 3). It falls in the foidite field of the total alkalis–silica (TAS) diagram (Le Maitre 2002), and the presence of modal and normative (14 wt%) nepheline together with the dominance of clinopyroxene as phenocrysts define this rock as a pyroxene-nephelinite. The total alkali content is high (4–5 wt%) for a relatively low SiO_2 content (39 wt%). The high Mg-number (63–64) of the nephelinite confirms its primitive character compared with the whole series of the Saghro volcanic field (Ibhi *et al.* 2002, and our unpublished data).

Quantitative textural analysis: crystal size distribution of clinopyroxene

Methods

The crystal size distribution (CSD) analysis was made on thin-section photomicrographs obtained with an optical microscope. The crystals were outlined using computer-aided design software and the drawing was exported as a black and white bitmap file. The size of the phenocrysts was measured with the 'SPO' software (Launeau 2004; Launeau & Robin 2005). With this method, each grain of the digitalized thin section is positioned, outlined and represented by an ellipse and a box (inertia tensor method). The measure used for the CSD analysis is the length of the ellipse major axis for each grain (200–500 grains per sample; the smallest measured grains are in the range 0.15–0.2 mm). The CSD 2D size data from the binary image were converted into volume data by applying stereological corrections based on the Schwartz–Saltikov algorithm (De Hoff & Rhines

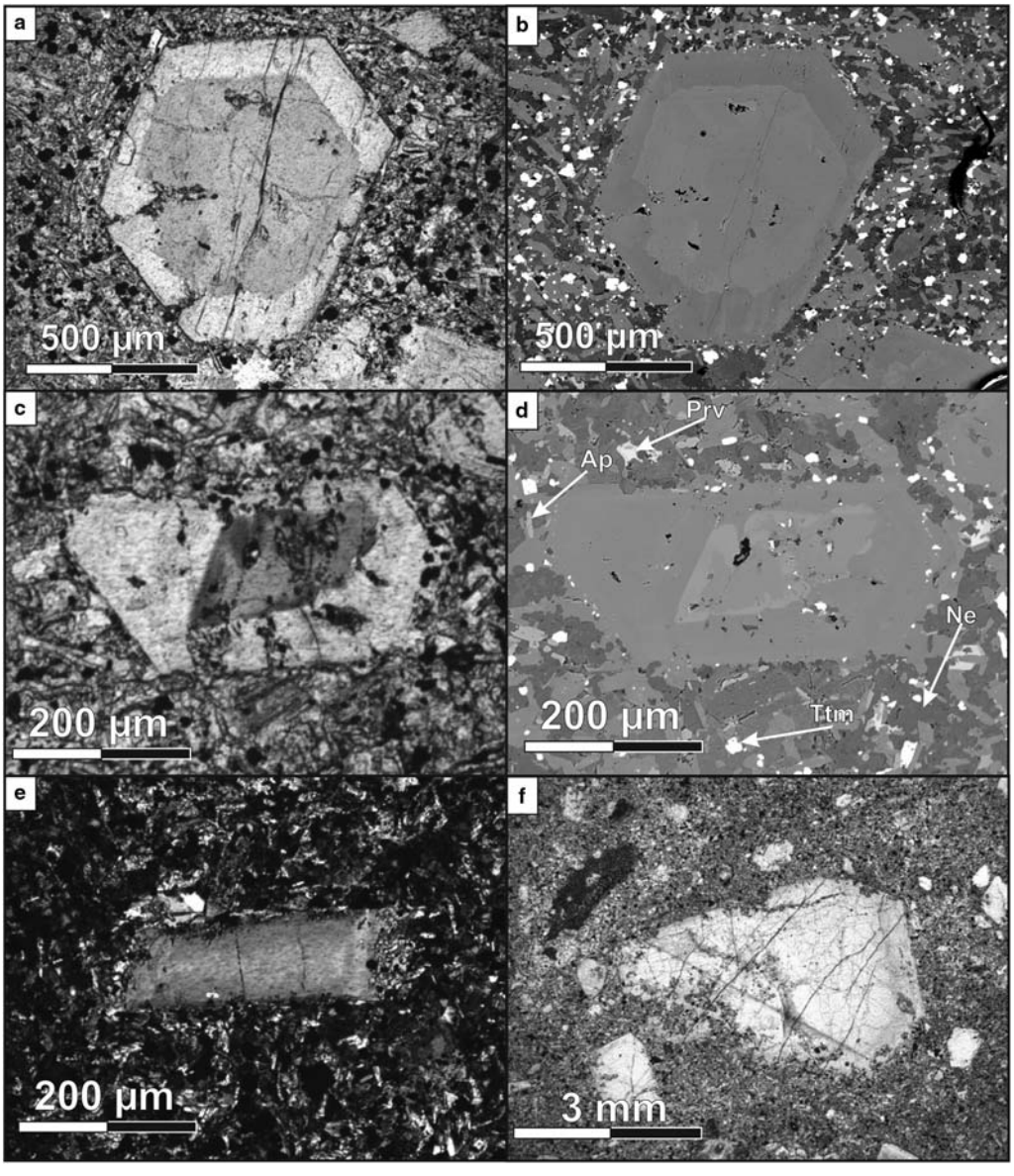

Fig. 2. Photomicrographs of clinopyroxenes. (**a**, **b**) Type 1: Ti-augite with brown Al-rich core: (a) transmitted light; (b) backscattered electron image. (**c**, **d**) Type 2: Ti-augite phenocryst with Fe-rich green core (c) transmitted light; (d) backscattered electron image. (**e**) Type 3: Ti-augite in plane-polarized light. (**f**) Transmitted light photomicrograph of a broken megacryst. Ne, nepheline; Ap, apatite; Ttm, titanomagnetite; Prv, perovskite.

1972). This procedure (Hammer *et al.* 1999) does not cause artefacts such as the pronounced reduction of the scatter of data observed for the method proposed by Peterson (1996). Stereological corrections based on the Schartz–Saltikov algorithm, as adopted by Armienti *et al.* (1994) and Higgins (2000), have been carefully tested against real and theoretical cases; they represent a satisfactory solution in most cases of petrological investigation. The CSD parameters used in this work were obtained using the software 'CSDcorrection1.36' (Higgins 2000, 2002).

The data were plotted, following general convention (Marsh 1988), as linear crystal

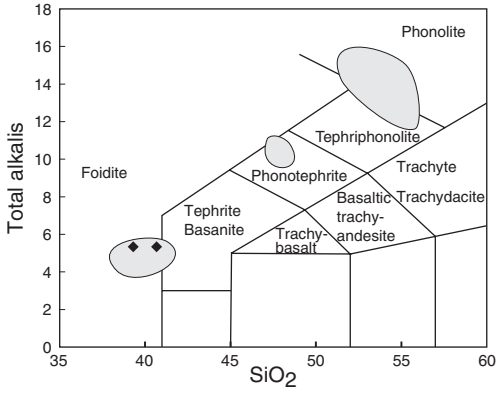

Fig. 3. TAS diagrams (fields from Le Maitre 2002) showing the composition of two analysed samples from the pyroxene-nephelinite flow. Grey fields indicate the composition of the whole Saghro lava suite (Ibhi 2000, and our unpublished data).

size v. population density (ln(n) (cm^{-4}) v. L (cm)); a $\log_{10}$ based scale with 4–8 bins per decade was used. Ten samples from the core and the lower border of the flow were selected for this purpose. The main parameters of the CSD analysis on these samples are shown in Table 1.

Results

Most of the plotted CSDs for the clinopyroxenes are straight or slightly curved but, in detail, three types of distribution can be recognized: (1) six samples have straight to slightly concave-upward curved CSD patterns (Fig. 4a); (2) three samples have a more pronounced curvature (Fig. 4b): the CSD is straight for the small crystals (<0.1 cm, corrected grain size) and shows a pronounced concave-upward pattern for larger grains (>0.1 cm); (3) one sample has a 'kinked' CSD pattern (Fig. 4c) characterized by a steep slope for smaller grains (<0.1 cm) and a more gentle slope for larger sizes (>0.1 cm), with a gap between the two populations.

The curved CSDs are best interpreted as mixing of two populations of crystals with contrasted crystallization histories. Higgins (1996) and Peterson (1996) have shown that mixing of two populations of crystals, each characterized by contrasting slopes in CSD patterns, can produce a slightly curved CSD. The kinked CSD pattern presented in Figure 4c can be divided into two parts: a slightly concave-upward curve similar to the curved CSD presented above and a population of large crystals identified as broken megacrysts. The first concave population, with a steep negative slope in the CSD diagram, is rich in small grains. It corresponds to the tabular euhedral unzoned small phenocrysts (type 3) mixed with small amounts of type 1 and 2 phenocrysts. The regressed CSD line of the slightly concave-upward curve has a slope between -43 and $-96\ cm^{-1}$ and an intercept between 12.5 and 16.2 cm^{-4}. The population of large clinopyroxenes, with a more gentle negative slope has a lower intercept, corresponds to a few large clinopyroxenes interpreted as megacrysts that show the same composition as type 1 phenocrysts. The CSD analysis of the few large crystals with kinked CSD patterns gives a slope around $-30\ cm^{-1}$.

The regressed slope and intercept of all CSDs are negatively correlated (Table 1). In a classic CSD diagram the regressed lines define a fan (not shown here; Resmini 1993; Zieg & Marsh 2002). However, following Higgins (2002), this correlation is not necessarily meaningful, because of the closure limit effect, and a diagram of characteristic length v. clinopyroxene modal proportion would give more information on geological processes. CSD regression parameters calculated on straight CSDs and small (usually <0.1 cm) clinopyroxene populations of curved and kinked

Table 1. *Results of CSD analysis on clinopyroxenes from the 10 analysed samples from the pyroxene-nephelinite flow of Foum el Kous*

Sample	Type	Intercept (cm^{-4})	1σ	Slope (cm^{-1})	1σ	Cpx vol% measured	Cpx vol% regressed
Fn3	*Curved*	14.42	0.17	−58.6	2.9	18.0	24.9
Fs1	*Straight*	14.42	0.18	−65.5	3.6	14.9	20.5
Fs6	*Straight*	12.40	0.22	−43.3	3.2	11.4	14.2
Fs10	*Kinked*	13.48	0.20	−48.9	3.3	17.0	10.0
Fs14	*Straight*	15.17	0.14	−67.0	3.0	18.1	27.1
Fs15	*Curved*	16.27	0.24	−92.3	6.6	17.8	21.2
Fs17	*Straight*	14.40	0.18	−63.5	3.9	18.3	22.8
Fs29	*Straight*	13.22	0.20	−47.5	3.1	16.1	21.5
Fs41	*Curved*	15.81	0.15	−86.1	4.0	21.1	29.2
Fs43	*Straight*	16.20	0.17	−95.7	5.2	21.0	26.5

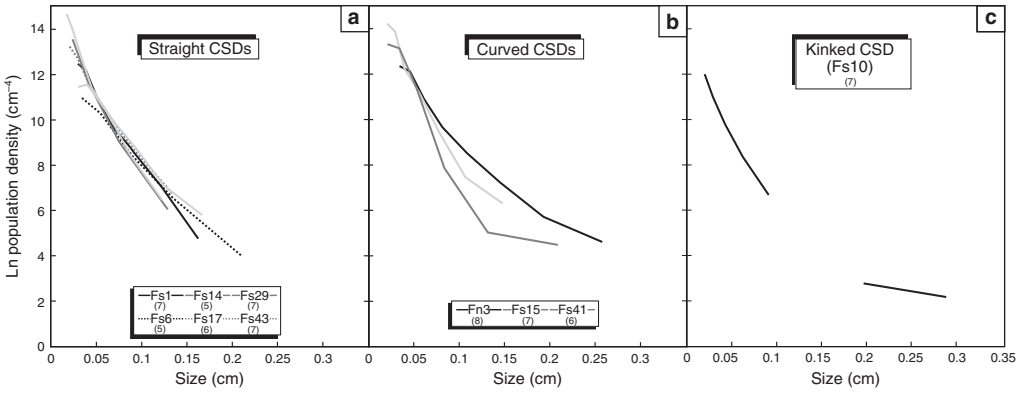

Fig. 4. The three types of CSD patterns observed for the clinopyroxenes of the pyroxene-nephelinite lava flow from Foum el Kous.

CSDs are plotted in Figure 5. The characteristic length of augite phenocrysts is negatively correlated with the modal proportion. The samples from the base of the flow have the highest clinopyroxene content (17–22 vol%) but generally low characteristic length (<0.013 cm).

Mineral chemistry: focus on clinopyroxene

The data have been acquired on a Cameca SX100 electron microprobe at the CAMPARIS section of the Paris VI University. The operating conditions were 10 nA for the beam current, 15 kV for the accelerating voltage and 10 s counting time per element. Corrections of the raw data were made using the PAP method of Pouchou & Pichoir (1984). Typical accuracy is close to 1% for oxides with concentration >1 wt% and around 10 wt% for elements with contents <1%.

Unzoned olivine phenocrysts have Mg-numbers between 82 and 87 for the entire flow. Groundmass nepheline shows a restricted compositional range of $Ne_{68-73}Ks_{26-31}Q_{0-3}$ and the Ti-magnetite has 11–16 wt% of TiO_2 with rather high MnO and MgO contents (1–2 and 3–6 wt%, respectively). Minor amounts of Nb–Zr–REE-rich perovskite and fluorapatite are present in the groundmass but they have not been quantitatively analysed.

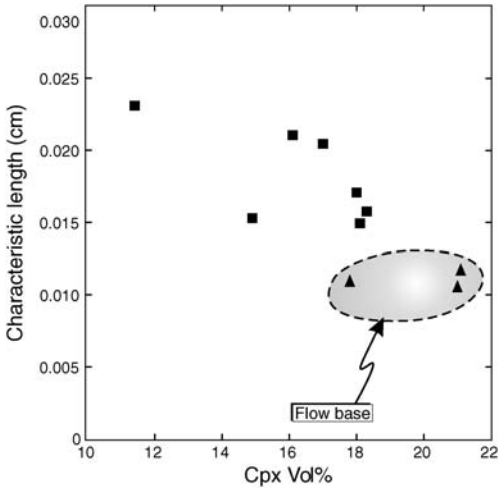

Fig. 5. Characteristic length v. clinopyroxene content (vol%) for straight CSDs and the left, straight, part of curved and kinked CSDs.

The clinopyroxene chemistry

The chemistry of the Saghro clinopyroxenes (Table 2; Fig. 6) is directly linked to their aspect and texture. The dark brown cores (type 1) are Ti- and Al-rich augite that can be distinguished by their high Al and Ti content, high $^{VI}Al/^{IV}Al$ ratio and rather low Mg-number (65–82). This compositional range is the same as those of the megacrysts and the clinopyroxene in pyroxenite xenoliths. Their high Al (0.3–0.5 p.f.u.) content and $^{VI}Al/^{IV}Al$ ratio point to a high pressure of crystallization (Aoki & Shiba 1973). These pyroxenes also have low Cr_2O_3 contents (<0.33 wt% Cr_2O_3), similar to high-pressure pyroxenes from alkaline lavas (Schulze 1987). The small unzoned euhedral phenocrysts (type 3) and the light brown mantle surrounding green and brown cores have the same composition with low Al and Ti contents but with a higher mean Mg-number (range 75–83) than the brown Ti–Al augite cores (type 1); their $^{VI}Al/^{IV}Al$ ratio is low (<0.3), indicating a lower crystallization pressure. The compositional differences between the brown cores and their

Table 2. *Representative analyses of clinopyroxene phases from the Foum el Kous pyroxene-nephelinite flow*

Sample:	Fs10	Fs17	Fs29	Fn3	Fs5	Fs10	Fs5	Fs10	Fs17	Fs5	Fs10	Fs29
Type:	Type 1	Type 1	Type 1	Type 2	Type 2	Type 2	Type 3	Type 3	Type 3	Type 4	Type 4	Type 4
Core/rim:	Core	Core	Core	Core	Core	Core	Core	Core	Core	Core	Core	Core
wt%												
SiO_2	46.11	44.26	43.74	39.45	42.82	43.80	47.28	44.84	47.67	50.91	49.99	47.20
TiO_2	2.55	2.89	3.35	3.98	3.36	2.96	2.09	2.93	2.33	2.06	2.19	3.17
Al_2O_3	8.68	10.91	10.59	14.95	11.58	9.27	7.74	8.59	6.02	2.64	3.36	4.83
Cr_2O_3	0.00	0.06	0.01	0.01	0.00	0.00	0.09	0.37	0.12	0.00	0.00	0.00
FeO	8.12	7.93	7.88	12.26	10.11	8.92	5.40	6.17	6.26	5.75	5.77	6.00
MnO	0.10	0.03	0.13	0.11	0.18	0.12	0.07	0.14	0.07	0.19	0.17	0.16
MgO	11.29	10.53	10.66	6.29	9.27	10.58	13.59	12.30	13.76	14.77	14.26	13.36
CaO	22.74	22.86	22.65	22.50	22.61	24.22	22.87	23.04	23.92	24.14	23.98	23.54
Na_2O	0.53	0.47	0.47	0.97	0.93	0.48	0.63	0.85	0.56	0.50	0.55	0.79
Sum	100.13	99.96	99.49	100.52	100.86	100.35	99.75	99.24	100.71	100.96	100.28	99.05
Structural formulae based on 6 oxygens, Fe^{3+} calculated by local charge balance												
Si	1.72	1.65	1.64	1.49	1.59	1.63	1.74	1.67	1.75	1.86	1.84	1.76
Al^{IV}	0.28	0.35	0.36	0.51	0.41	0.37	0.26	0.33	0.25	0.11	0.15	0.21
Al^{VI}	0.10	0.13	0.11	0.16	0.10	0.04	0.08	0.05	0.01	0.00	0.00	0.00
Fe^{3+}	0.08	0.08	0.09	0.19	0.18	0.19	0.11	0.17	0.15	0.06	0.08	0.12
Ti	0.07	0.08	0.09	0.11	0.09	0.08	0.06	0.08	0.06	0.06	0.06	0.09
Cr	0.00	0.00	0.00	0.00	0.00	0.00	0.00	0.01	0.00	0.00	0.00	0.00
Mg	0.63	0.59	0.60	0.35	0.51	0.59	0.75	0.68	0.75	0.80	0.78	0.74
Fe^{2+}	0.17	0.16	0.16	0.19	0.13	0.09	0.06	0.02	0.04	0.09	0.08	0.04
Mn	0.00	0.00	0.00	0.00	0.01	0.00	0.00	0.00	0.00	0.01	0.01	0.00
Ca	0.91	0.91	0.91	0.91	0.90	0.97	0.90	0.92	0.94	0.94	0.95	0.94
Na	0.04	0.03	0.03	0.07	0.07	0.03	0.04	0.06	0.04	0.04	0.04	0.06
Mg-no.	0.71	0.70	0.71	0.48	0.62	0.68	0.82	0.78	0.80	0.84	0.83	0.82

(*Continued*)

Table 2. *Continued*

Sample:	Fn3	Fs10	Fs17	Fs10	Fs17	Fs29	Fs17	Fs17	Fs17	Fs3	Fs3	Fs3
Type:	Light mantle	Light mantle	Light mantle	Rim	Rim	Rim	Megacryst	Megacryst	Megacryst	Xenolith	Xenolith	Xenolith
Core/rim:	Rim	Rim	Rim	Rim	Rim	Rim	Core	Core	Core	Core	Core	Core
wt%												
SiO_2	48.11	48.44	46.97	53.66	50.12	50.41	47.27	43.53	48.27	44.96	46.71	48.61
TiO_2	2.10	1.82	2.58	0.89	2.21	2.09	2.11	3.41	1.75	2.65	1.78	1.85
Al_2O_3	5.98	5.40	5.82	0.46	3.47	2.73	8.01	9.10	7.04	9.92	8.08	6.34
Cr_2O_3	0.15	0.00	0.00	0.02	0.08	0.01	0.39	0.05	0.41	0.05	0.20	0.22
FeO	6.04	6.82	6.15	4.36	5.55	5.30	4.43	7.14	4.27	6.71	6.05	5.42
MnO	0.08	0.11	0.18	0.14	0.12	0.15	0.01	0.12	0.09	0.04	0.04	0.08
MgO	14.01	13.27	13.59	15.83	14.38	14.61	13.37	11.71	14.12	11.72	12.89	13.77
CaO	23.32	23.19	24.34	24.30	24.41	24.36	23.11	23.41	23.01	22.47	23.16	22.82
Na_2O	0.53	0.61	0.38	0.56	0.43	0.59	0.57	0.52	0.50	0.74	0.51	0.61
Sum	100.33	99.67	100.02	100.24	100.77	100.25	99.27	98.99	99.48	99.27	99.42	99.74
Structural formulae based on 6 oxygens, Fe^{3+} calculated by local charge balance												
Si	1.77	1.80	1.74	1.96	1.84	1.85	1.75	1.64	1.78	1.68	1.73	1.79
Al^{IV}	0.23	0.20	0.25	0.02	0.15	0.12	0.25	0.36	0.22	0.32	0.27	0.21
Al^{VI}	0.03	0.03	0.00	0.00	0.00	0.00	0.10	0.04	0.08	0.11	0.09	0.07
Fe^{3+}	0.12	0.11	0.15	0.03	0.07	0.07	0.06	0.17	0.06	0.12	0.11	0.07
Ti	0.06	0.05	0.07	0.02	0.06	0.06	0.06	0.10	0.05	0.07	0.05	0.05
Cr	0.00	0.00	0.00	0.00	0.00	0.00	0.01	0.00	0.01	0.00	0.01	0.01
Mg	0.77	0.73	0.75	0.86	0.79	0.80	0.74	0.66	0.78	0.65	0.71	0.76
Fe^{2+}	0.06	0.10	0.03	0.09	0.09	0.06	0.07	0.05	0.07	0.09	0.08	0.09
Mn	0.00	0.00	0.01	0.00	0.00	0.00	0.00	0.00	0.00	0.00	0.00	0.00
Ca	0.92	0.92	0.96	0.95	0.96	0.96	0.92	0.94	0.91	0.90	0.92	0.90
Na	0.04	0.04	0.03	0.04	0.03	0.04	0.04	0.04	0.04	0.05	0.04	0.04
Mg-no.	0.81	0.78	0.81	0.88	0.83	0.86	0.84	0.75	0.85	0.76	0.79	0.82

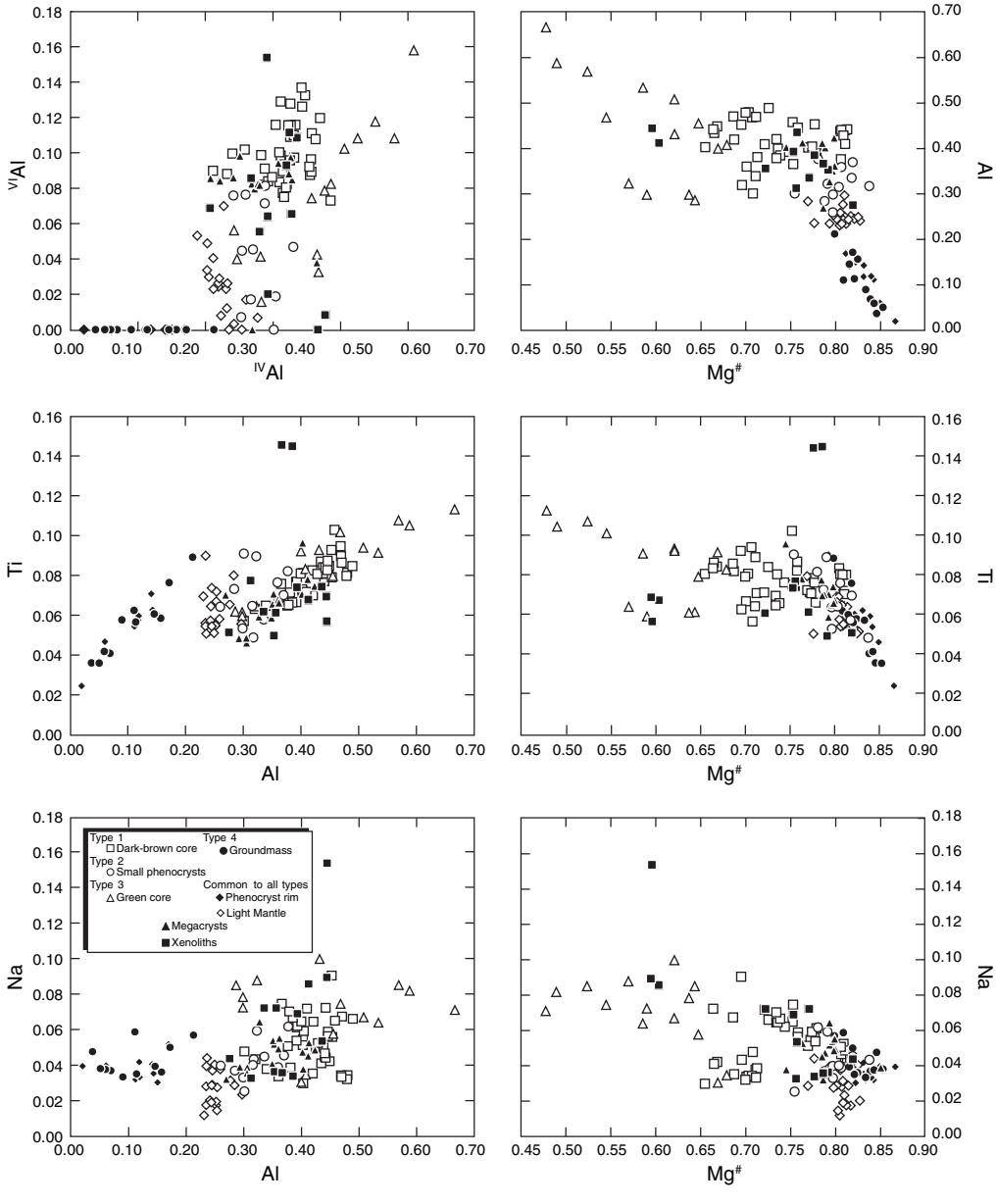

Fig. 6. Composition of the clinopyroxenes from the pyroxene-nephelinite flow of Foum el Kous.

surrounding light mantles for type 1 clinopyroxene are illustrated by a microprobe traverse (Fig. 7a): there is a drastic increase of Mg content and a concomitant drop in Al and Fe contents from the core to the mantle zone. Na and Ti contents do not vary significantly in the two parts of the phenocrysts. The zoned clinopyroxene with green core (type 3) has a slightly higher Fe content than the other pyroxenes; it corresponds to an Al–Fe augite. The Mg-number is low (45–65) whereas the Na, Al and Ti contents are high (>0.3, 0.03–0.1 and 0.06–0.12 p.f.u., respectively). Here also, the high $^{VI}Al/^{IV}Al$ ratio is indicative of a high pressure of crystallization. A close examination of the microprobe traverse (Fig. 7b) shows that four zones are present: a green core with 0.3–0.4 p.f.u. Fe, a green external core characterized by much higher Fe and Al contents (both up to 0.5 p.f.u.), a light

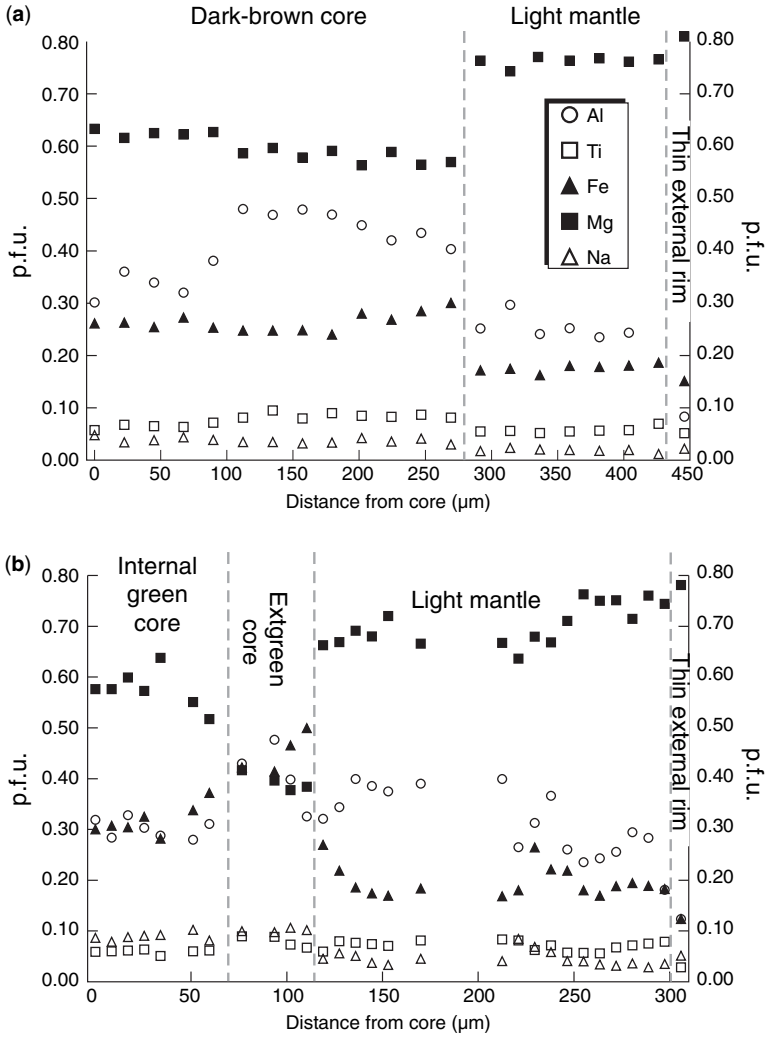

Fig. 7. Microprobe traverses within the clinopyroxene phenocrysts with brown core (type 1: **a**) and green core (type 2: **b**).

large brown mantle with lower Al but higher Mg contents, and a thin (<20 μm) rim with extremely low Al but high Mg. The composition of the groundmass clinopyroxene overlaps those of the extreme rims of the phenocrysts. They have the lowest Al, Ti and ^{VI}Al contents but the highest Mg-number (78–87).

Thermobarometry

Two methods have been used here to quantitatively estimate the crystallization pressure.

The first method is the structural barometer of Nimis & Ulmer (1998); this has the advantage of being composition independent and avoids the problems of cpx–melt disequilibrium. Exact knowledge of the equilibrium melt composition is not required but the type of melt has to be known (anhydrous v. hydrous, tholeiitic v. alkaline, etc.). The presence of hydrated minerals (amphibole and biotite) in the megacrysts and in the xenoliths together with the 2.5 wt% value of the whole-rock loss on ignition (LOI) argue for a significant water content of the parental magma. In consequence, the barometer calibrated for hydrous basaltic compositions has been used (the anhydrous calibration was tested but the results were significantly too low, <5 kbar).

The second method is the barometer based on clinopyroxene–liquid equilibrium (Putirka *et al.* 2003); it was not applied to phenocrysts with Mg-number <70 because of evident disequilibrium

with the nephelinite melt composition. In this barometer, the relation between the composition and the pressure was established by minimizing the Gibbs free energy at equilibrium, assuming an ideal behaviour of the components. This barometer covers a wide compositional range, from silica-undersaturated to silicic melts, including alkali-rich lavas. However, it requires an independent estimation of the temperature. For that purpose, the pyroxene solvus thermometer of Lindsley (1983) was used. As the content of non-quadrilateral components (Al, Ti, Na) is high in the Saghro clinopyroxenes, the error on the temperature calculation is >50 °C (Lindsley 1983), approaching 100 °C (the error increase is about 5 °C per mol% of non-quadrilateral components).

For the pyroxene megacrysts, the pyroxenes of the xenoliths and the dark brown cores of phenocrysts (type 1), the data cluster between 1000 and 1200 °C, with most values between 1100 and 1200 °C. This result is consistent with those of previous studies on clinopyroxenes from alkaline lavas (Bondi *et al.* 2002; Damasceno *et al.* 2002). The light mantle overgrowths and the small phenocrysts (types 2 and 3) have crystallization temperatures in the same range, or slightly lower, around 1100 °C. The groundmass pyroxenes (type 4) and the rims of phenocrysts have crystallized at significantly lower temperatures, below 1000 °C, with a mean value close to 950 °C.

Concerning pressure, to handle the large number of values calculated and taking into account the large errors inherent in the geobarometers used (±2.6 kbar, according to Nimis & Ulmer 1998) the results have been treated statistically. Histograms of crystallization pressures are presented in Figure 8 for the two barometers.

Pressure estimates from the structural barometer for the dark brown cores of type 1 clinopyroxene, green cores of type 2, megacrysts and xenoliths range between 7 and 14 kbar, with a peak between 9 and 10 kbar (mean 9.9 ± 1.6 kbar; the presented error is the standard deviation on the population of measured pressures).

The light mantle surrounding the core of phenocrysts and the small phenocrysts (type 3) have crystallization pressures between 3 and 9 kbar, with a peak between 5 and 6 kbar (mean 5.9 ± 1.9 kbar). The cpx–liquid barometer (Putirka *et al.* 2003) gives a slightly lower mean value (mean 4.6 ± 1.5 kbar), but this is similar within error limits to type 3 clinopyroxenes, although the distribution appears to be bimodal with one cluster between 3 and 4 kbar and another between 6 and 7 kbar. Groundmass clinopyroxene and the phenocryst rims (type 4) have significantly lower crystallization pressure (0–4 kbar) with a mean of 1 ± 1.1 kbar. In detail, the crystallization pressure of the type 4 pyroxenes also seems to be bimodal, with one cluster around 0 kbar (surface conditions) and another between 2 and 3 kbar. The calibration of Putirka *et al.* (2003) either gives low values (<2 kbar) for groundmass clinopyroxene (type 4) or is unable to calculate a pressure. This is due to the very low content in the jadeite end-member (close or equal to zero) in the groundmass pyroxenes.

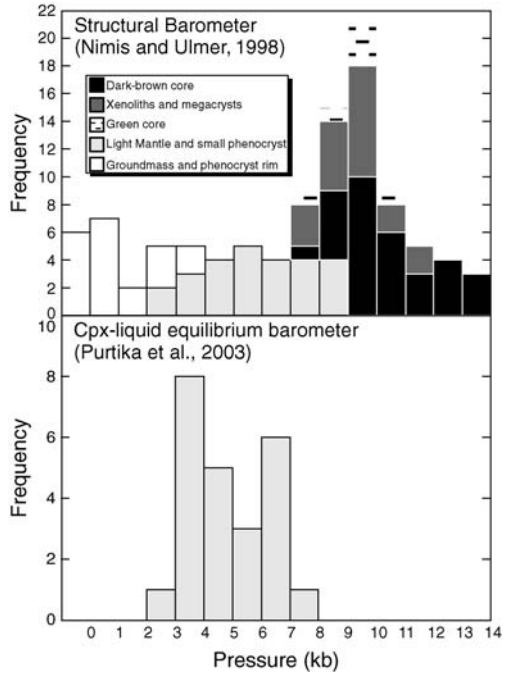

Fig. 8. Histograms of pressure estimates for the different types of clinopyroxene from the nephelinite flow.

Discussion

Polybaric differentiation and the level of magma chambers

The high-Al augite (cores of type 1 and 2) of the nephelinite flow is characterized by high $^{VI}Al/^{IV}Al$ ratio and has generally the same composition as the pyroxenes from the xenoliths and the megacrysts. Pressure estimates for these clinopyroxenes are around 10 kbar, but a higher pressure has been obtained for one sample (up to 14 kbar). The geophysical modelling of the Anti-Atlas lithosphere (Teixell *et al.* 2005) has revealed a crustal thickness of 36 km. Considering a density of 2750 kg m^{-3} for the upper crust and 2930 kg m^{-3} for the lower crust and respective thicknesses of 23 and 13 km (Teixell

et al. 2005), the calculated pressure is 6.1 kbar at the base of the upper crust and 9.8 kbar at the crust–mantle boundary. The high-Al augite thus represents fractionation products of the nephelinite magma in a magma chamber located close to the Moho. Some megacrysts may even have crystallized at higher pressure (*c.* 14 kbar) in the mantle at a depth of about 50 km. Considering that the base of the lithospheric mantle is at *c.* 60–70 km (Teixell *et al.* 2005), this depth could correspond to the depth at which the lithospheric mantle becomes ductile; that is, at the transition between the mechanical boundary layer and the thermal boundary layer (MBL–TBL transition).

Crystallization pressure of the small phenocrysts (type 3) and of the light mantle surrounding high-Al cores are around 6 kbar, a pressure that closely corresponds to the depth of the upper–lower crust boundary. We can then ascribe a second magma chamber to this physical boundary (Fig. 9). The low-Al augites from the groundmass and the thin rims of the phenocrysts have crystallized at very low pressure (0–1 kbar), in a subvolcanic magma chamber or at the surface, after eruption of the nephelinite flow. The *P* estimates summarized in Figure 8 seem to suggest a continuous range of pressure from 14 to 0 kbar for clinopyroxene crystallization instead of the three discrete stages as discussed above. However, a close examination of the phenocryst zonations shows that the contacts between the zones are sharp from both the chemical and optical points of view. Pressure computed from the composition along a microprobe traverse in a type 1 phenocryst also shows that the core has crystallized at high pressure (10 kbar) and the mantle at about 5–6 kbar with no intermediate value. The apparent continuous pressure range is thus most probably an effect of the uncertainties inherent in the structural barometer ($\pm$2.6–3.0 kbar; Nimis & Ulmer 1998) and in analytical errors. We can thus infer the presence of magma chambers at three or maybe four structural levels beneath the Djbel Saghro volcanic system: just below the surface, at the upper–lower crust boundary, at the crust–mantle boundary, and possibly within the lithospheric mantle, at the MBL–TBL boundary. However, whether there are several magma chambers or only one at each structural level for the Saghro volcanic field as a whole (1500 km^2) has not yet been assessed.

Evidence for multi-chamber magmatic differentiation is common in alkaline volcanic series (Woodland & Jugo 2007). Beneath the Sirwa volcano (Bondi *et al.* 2002), the high-Al diopside is thought to have crystallized in a deep magma chamber, at the crust–mantle boundary. In the

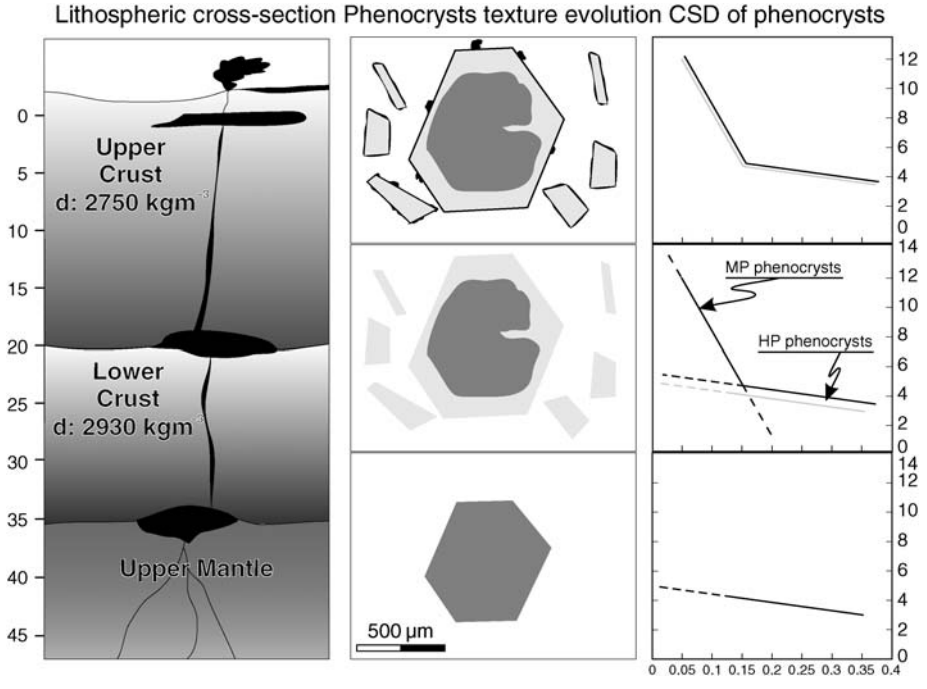

Fig. 9. Schematic sketch representing the location of the magma chambers in the lithospheric cross-section, the textural evolution of the clinopyroxene phenocrysts during their ascent to the surface and the related CSD patterns.

Kerguelen archipelago, a detailed study of clinopyroxenes has revealed three magma chambers emplaced at the levels of the physical boundaries in the crust (Damasceno *et al.* 2002). This is also the case for the Saghro lavas.

The interaction between the Mg-rich mantle-derived nephelinite and a phonolitic melt at the base of the crust probably enhanced the rapid ascent of the mafic melt towards the magma chamber situated at the Conrad discontinuity (Woodland & Jugo 2007). The mixing between two magmas of contrasted compositions presumably led to the uptake of the differentiated Al- and Fe-rich phenocrysts and megacrysts from the phonolitic magma chamber in the nephelinite magma.

In areas for which geophysical data are not available, this barometric approach on clinopyroxenes could be a powerful tool to estimate the depth of the most important interfaces within the lithosphere, in active or recently extinct volcanic fields.

CSD analysis: evidence for magma mixing and crystal settling

The CSD of clinopyroxene phenocrysts shows three types of patterns. Samples with straight CSDs are devoid of high pressure (HP; *c.* 10 kbar) crystals. Curved and kinked CSDs are a mixture between two populations of clinopyroxene: (1) types 1 and 2 pyroxenes with Fe- and Al-rich cores that crystallized at around 10 kbar and (2) type 3 Mg-rich brown augite forming either light mantles around high-pressure cores or unzoned phenocrysts (or megacrysts) that crystallized at medium pressure (MP; *c.* 0.6 kbar). The population of MP phenocrysts (population A, Fig. 9) has a steep slope in CSD diagrams whereas pyroxenes with HP cores (population B) have CSDs with more gentle slopes. In CSD diagrams (Figs 4 and 9), the transition between the two populations corresponds to a size around 0.1 cm. The difference between the curved and the kinked CSDs probably results from the different percentages of the two populations in a given sample and from the contrast of size between the two CSD populations. In fact, the transition between the two CSD populations is progressive; there is a continuous range of grain sizes. Following Higgins (1996) and Peterson (1996), a curved CSD would correspond to a mixture of population A grains (type 1 pyroxene) with only a small amount (1–5 vol%) of population B grains (type 1 and 2 phenocrysts). The kinked CSD represents samples in which only a few very large crystals (broken megacrysts, up to 0.4 cm) with HP cores are present in a matrix of smaller MP phenocrysts. The gap between the two parts of the kinked CSD represents the lack of crystals with intermediate sizes (0.1–0.25 cm). Similar conclusions have already been drawn on textural analysis of megacryst-bearing granitoids (Higgins 1999). Even if only three large crystals are present, they account for a significant part of the CSD because they occupy a large modal volume (up to 7 vol%), forming their own CSD with a gentle slope. The CSDs in our samples are the witness of an important process of crystal mixing of two populations with contrasted composition and pressure of crystallization (Fig. 9).

The steeper CSD (measured on clinopyroxene populations <0.1 cm) of the three samples collected at the base of the flow cannot be explained as the result of faster cooling rates at the base of the flow (Zieg & Marsh 2002) because clinopyroxene phenocrysts were already present in the magma before eruption (the small phenocrysts have crystallized at around 6 kbar). Moreover, the Bagnold effect cannot account for the steeper slope and high modal proportions observed in the lowermost samples, because this will displace most of the crystals toward the core of the flow, where magma velocities are higher (Nkono *et al.* 2006, and references therein). As a result, the base of the flow will be crystal poor and this does not fit with our observations. We propose that the higher clinopyroxene modal proportions towards the base of the flow are the result of crystal settling during cooling of the nephelinite flow at the surface; such observations have already been made at the base of thick andesitic flows (Higgins 2002).

Evidence for mixing between phonolite and nephelinite

A characteristic of the studied nephelinite flow is the wide compositional range of its pyroxenes. The high variability of clinopyroxene Mg-number (48–88) suggests that most of them are in disequilibrium with the host nephelinite liquid. Fe–Mg exchange coefficients between clinopyroxene and liquid (K_d) vary from 0.1 to 0.49 in most crystallization experiments (0.01–110 kbar; 800–1800 °C in basic to silicic melts; Putirka *et al.* 2003). An average K_d value of 0.27 ± 0.06 is in agreement with most experiments (Putirka *et al.* 2003; see references given by Scoates *et al.* 2006). The pyroxenes in equilibrium with the Saghro nephelinite liquids (Mg-number 62–70) should have an Mg-number between 80 and 92. This implies that the pyroxenes with Mg-number <80 have crystallized from more evolved Fe-rich melts. Only the groundmass pyroxene, the rim of the phenocrysts and the small euhedral unzoned phenocrysts

(including the light mantle overgrowths surrounding the HP cores) seem to be in equilibrium with the host rock. The green augite forming the core of some clinopyroxene phenocrysts (types 1 and 2) is also too Fe-rich to be in equilibrium with the nephelinite. As no other peralkaline magmatic activity is documented in the area, the low Mg but Fe- and Al-rich green augite cannot be a xenocryst from the surrounding rocks and must be contemporaneous with the nephelinite magmatism. Its low Mg-number suggests that it was probably in equilibrium with a phonolitic liquid (Fig. 10). The brown high-Al Ti-augite forming the core of some phenocrysts as well as pyroxene megacrysts and those from pyroxenite xenoliths have a composition intermediate between the augite from the phonolite and that from the nephelinite. We can conclude that these phenocrysts have crystallized from a melt that probably formed by mixing of a phonolite and a nephelinite. Indeed, only one exposure of intermediate magma has been found in the Saghro area and field evidence (presence of mafic volcanic enclaves in a more felsic matrix) suggests that this lava was formed through the mechanical mixing between two different magmas. Such a model is reasonable, as magma mixing is also thought to play an important role in the genesis of the nephelinite–phonolite bimodal associations (Duda & Schmincke 1985; Gwalani *et al.* 2000). The nephelinite magma has been mixed with a more evolved melt of phonolitic composition at the level of the Moho discontinuity. There is thus a need for a magma chamber of phonolitic composition at the Moho. The first clinopyroxene in equilibrium with the nephelinite (type 3 pyroxene represented by population A in CSDs) crystallized only at 6 kbar, at the upper–lower crust interface. The interaction between the nephelinite magma and the phonolitic magma probably produced rapid ascent of the nephelinite melt towards the lower–upper crust boundary, where it began to crystallize MP, Mg-rich clinopyroxene phenocrysts. Magma mixing is indeed one of the proposed factors to explain rapid ascent of magma from a deeper level; it thus allows the uptake of xenocrysts, megacrysts and xenoliths to the surface (Woodland & Jugo 2007).

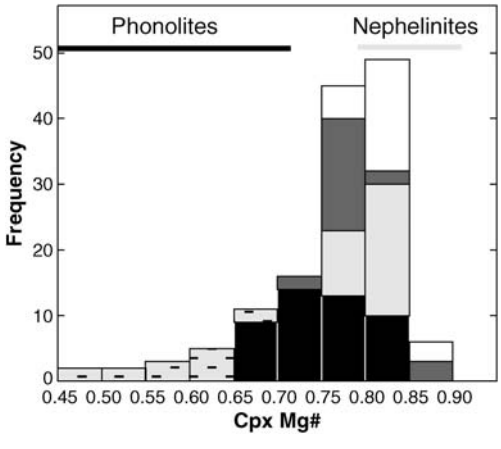

Fig. 10. Histogram showing the distribution of the clinopyroxene Mg-number in the pyroxene-nephelinite flow. The ranges labelled phonolites and nephelinites are the theoretical ranges of composition of clinopyroxenes in equilibrium with phonolites and nephelinites from the Saghro, considering a range for Fe–Mg exchange coefficient between 0.21 and 0.33. Legend as in Figure 8.

Conclusion

The crystal size distribution (CSD) of clinopyroxene phenocrysts in a single nephelinite flow of the Saghro volcanic field (Morocco) suggests that at least two populations of augite phenocrysts coexist. The curved and kinked CSD patterns can be modelled as the mixture of two straight CSDs: a population of small phenocrysts of brown clinopyroxene (<0.1 cm) and a population of large augites (>0.1 cm) characterized by dark brown to green cores. The thermobarometric investigations show that the two populations have not crystallized at the same depth. The first population comes from a magma chamber at the upper–lower crust boundary (6 kbar) and the second population corresponds to the relicts of the high-pressure fractionation of the magma, at the Moho discontinuity (10 kbar). In addition, a few crystals give a still higher pressure of 14 kbar, suggesting crystallization within the lithospheric mantle, at the MBL–TBL boundary. Groundmass clinopyroxene probably crystallized during flow emplacement but the existence of a subvolcanic chamber cannot be excluded.

The various clinopyroxenes observed in a single nephelinite flow indicate the presence of four magma chambers, each located at rheological discontinuities of the local lithosphere: (1) at the brittle–ductile transition within the lithospheric mantle; (2) at the mantle–crust transition; (3) at the brittle–ductile transition within the crust; (4) at the lithosphere–atmosphere transition. The pressure determined for these four structural levels (respectively 14, 10, 6 kbar and *c.* 1 kbar) is in agreement with geophysical modelling. In addition, these magma chambers are close to a vertical lithospheric structure corresponding to the transition between the northern boundary of the West African craton (Ennih & Liégeois 2001) and the Jurassic palaeorift of the High Atlas mountains.

The wide range of clinopyroxene compositions in a single nephelinite flow (Mg-number 48–88) and the mixing of the two crystal populations suggested by the CSD analysis demonstrate that magma mixing between a phonolitic melt and a nephelinitic melt plays an important role in the genesis of the Saghro bimodal peralkaline lava suite. The detailed approach that we use in this study is potentially applicable to many active volcanoes. It could be used to monitor active volcanic fields by investigating the depth of the subsurface and deep-seated magma reservoirs.

J.B. and N.E. thank the local Moroccan people from the Djbel Saghro area for their hospitality and help in the field. J.B. and D.D. also acknowledge the ULB 'Fonds Cambier' for financing field trips to Morocco. The helpful comments of M. D. Higgins and R. G. Resmini improved the quality of the paper.

References

AOKI, K. & SHIBA, I. 1973. Pyroxenes from lherzolite inclusion of Itinomegata, Japan. *Lithos*, **6**, 41–51.

ARMIENTI, P., PARESCHI, M. T., INNOCENTI, F. & POMPILIO, M. 1994. Effects of magma storage and ascent on the kinetics of crystal-growth—the case of the 1991–93 Mt Etna eruption. *Contributions to Mineralogy and Petrology*, **115**, 402–414.

BACHMANN, O. & DUNGAN, M. A. 2002. Temperature-induced Al-zoning in hornblendes of the Fish Canyon magma, Colorado. *American Mineralogist*, **87**, 1062–1076.

BERRAHMA, M., DELALOYE, M., FAURE-MURET, A. & RACHDI, H. 1993. Premières données géochronologiques sur le volcanisme alcalin du Jbel Saghro, Anti-Atlas, Maroc. *Journal of African Earth Sciences*, **17**, 333–341.

BONDI, M., MORTEN, L., NIMIS, P., ROSSI, P. L. & TRANNE, C. A. 2002. Megacrysts and mafic–ultramafic xenolith-bearing ignimbrites from Sirwa Volcano, Morocco: phase petrology and thermobarometry. *Mineralogy and Petrology*, **75**, 203–221.

DAMASCENO, D., SCOATES, J. S., WEIS, D., FREY, F. A. & GIRET, A. 2002. Mineral chemistry of mildly alkalic basalts from the 25 Ma Mont Crozier section, Kerguelen Archipelago; constraints on phenocryst crystallization environments. *Journal of Petrology*, **43**, 1389–1413.

DOBOSI, G. 1989. Clinopyroxene zoning patterns in the young alkali basalts of Hungary and their petrogenetic significance. *Contributions to Mineralogy and Petrology*, **101**, 112–121.

DUDA, A. & SCHMINCKE, H.-U. 1985. Polybaric differentiation of alkali basaltic magmas: evidence from green-core clinopyroxenes (Eifel, FRG). *Contributions to Mineralogy and Petrology*, **91**, 340–353.

ENNIH, N. & LIÉGEOIS, J. P. 2001. The Moroccan Anti-Atlas: the West African craton passive margin with limited Pan-African activity. Implications for the northern limit of the craton. *Precambrian Research*, **112**, 291–304.

GROVE, T. L. & BAKER, M. B. 1984. Phase equilibrium controls on the tholeiitic versus calc-alkaline differentiation trends. *Journal of Geophysical Research*, **89**, 3253–3274.

GWALANI, L. G., ROCK, N. M. S., RAMASAMY, R., GRIFFIN, B. J. & MULAI, B. P. 2000. Complexly zoned Ti-rich melanite–schorlomite garnets from Ambadungar carbonatite–alkalic complex, Deccan Igneous Province, Gujarat State, Western India. *Journal of Asian Earth Sciences*, **18**, 163–176.

HAMMER, J. E., CASHMAN, K. V., HOBLITT, R. P. & NEWMAN, S. 1999. Degassing and microlite crystallization during pre-climactic events of the 1991 eruption of Mt. Pinatubo, Philippines. *Bulletin of Volcanology*, **60**, 355–380.

HIGGINS, M. D. 1996. Magma dynamics beneath Kameni volcano, Thera, Greece, as revealed by crystal size and shape measurements. *Journal of Volcanology and Geothermal Research*, **70**, 37–48.

HIGGINS, M. D. 1999. Origin of megacrysts in granitoids by textural coarsening: a crystal size distribution (CSD) study of microcline in the Cathedral Peak granodiorite, Sierra Nevada, California. *In*: FERNANDEZ, C. & CASTRO, A. (eds) *Understanding Granites: Integrating Modern and Classical Techniques*. Geological Society, London, Special Publications, **158**, 207–219.

HIGGINS, M. D. 2000. Measurement of crystal size distributions. *American Mineralogist*, **85**, 1105–1116.

HIGGINS, M. D. 2002. Closure in crystal size distributions (CSD), verification of CSD calculations, and the significance of CSD fans. *American Mineralogist*, **87**, 171–175.

HOERNLE, K. & SCHMINCKE, H. U. 1993. The role of partial melting in the 15-Ma geochemical evolution of Gran Canaria—a blob model for the Canary hotspot. *Journal of Petrology*, **34**, 599–626.

IBHI, A. 2000. *Le volcanisme Plio-Quaternaire de Saghro (Anti-Atlas, Maroc) et les enclaves basiques et ultrabasiques associées*. PhD thesis, University of Agadir.

IBHI, A., NACHIT, H., ABIA, E. H. & HERNANDEZ, J. 2002. Intervention of carbonate components in the petrogenesis of the pyroxene nephelinites from the Jbel Saghro (Anti-Atlas, Morocco). *Bulletin de la Société Géologique de France*, **173**, 37–43.

LAUNEAU, P. 2004. Mise en évidence des écoulements magmatiques par analyse d'images 2-D des distributions 3-D d'orientations préférentielles de formes. *Bulletin de la Société Géologique de France*, **175**, 331–350.

LAUNEAU, P. & ROBIN, P.-Y. F. 2005. Determination of fabric and strain ellipsoids from measured sectional ellipses—implementation and applications. *Journal of Structural Geology*, **27**, 2223–2233.

LE MAITRE, R. W. 2002. *Igneous Rocks. A Classification and Glossary of Terms*, 2nd edn. Cambridge University Press, Cambridge.

LIÉGEOIS, J.-P., BENHALLOU, A., AZZOUNI-SEKKAL, A., YAHIAOUI, R. & BONIN, B. 2005. The Hoggar swell and volcanism: Reactivation of the Precambrian Tuareg shield during Alpine convergence and West African Cenozoic volcanism. *In*: FOULGER, G. R., NATLAND, J. H., PRESNALL, D. C. & ANDERSON, D. L. (eds) *Plates, Plumes and Paradigms*. Geological Society of America, Special Papers, **388**, 379–400.

LINDSLEY, D. H. 1983. Pyroxene thermometry. *American Mineralogist*, **68**, 477–493.

MARSH, B. D. 1988. Crystal Size Distribution (CSD) in rocks and the kinetics and dynamics of crystallization. 1. Theory. *Contributions to Mineralogy and Petrology*, **99**, 277–291.

NIMIS, P. & ULMER, P. 1998. Clinopyroxene geobarometry of magmatic rocks Part 1: An expanded structural geobarometer for anhydrous and hydrous, basic and ultrabasic systems. *Contributions to Mineralogy and Petrology*, **133**, 122–135.

NKONO, C., FEMENIAS, O., DIOT, H., BERZA, T. & DEMAIFFE, D. 2006. Flowage differentiation in an andesitic dyke of the Motru Dyke Swarm (Southern Carpathians, Romania) inferred from AMS, CSD and geochemistry. *Journal of Volcanology and Geothermal Research*, **154**, 201–221.

O'BRIEN, H. E., IRVING, A. J. & MCCALLUM, I. S. 1988. Complex zoning and resorption of phenocrysts in mixed potassic mafic magmas of the Highwood Mountains, Montana. *American Mineralogist*, **73**, 1007–1024.

PETERSON, T. D. 1996. A refined technique for measuring crystal size distributions in thin section. *Contributions to Mineralogy and Petrology*, **124**, 395–405.

POUCHOU, J. L. & PICHOIR, F. 1984. Un nouveau modèle de calcul pour la microanalyse quantitative par spectrométrie de rayons X—Partie I: application à l'analyse d'échantillons homogènes. *Recherche Aérospatiale*, **3**, 167–192.

PUTIRKA, K. D., MIKAELIAN, H., RYERSON, F. & SHAW, H. 2003. New clinopyroxene–liquid thermobarometers for mafic, evolved, and volatile-bearing lava compositions, with applications to lavas from Tibet and the Snake River Plain, Idaho. *American Mineralogist*, **88**, 1542–1554.

RESMINI, R. G. 1993. *Dynamics of Magma Within the Crust: A Study Using Crystal Size Distributions*. PhD dissertation, Johns Hopkins University, Baltimore, MD.

SCHULZE, D. J. 1987. Megacrysts from alkalic volcanic rocks. *In*: NIXON, P. H. (ed.) *Mantle Xenoliths*. Wiley, New York, 433–451.

SCOATES, J. S., LO CASCIO, M., WEIS, D. & LINDSLEY, D. H. 2006. Experimental constraints on the origin and evolution of mildly alkalic basalts from the Kerguelen Archipelago, Southeast Indian Ocean. *Contributions to Mineralogy and Petrology*, **151**, 582–599.

STRECK, M. J., DUNGAN, M. A., MALAVASSI, E., REAGAN, M. K. & BUSSY, F. 2002. The role of basalt replenishment in the generation of basaltic andesites of the ongoing activity at Arenal volcano, Costa Rica: evidence from clinopyroxene and spinel. *Bulletin of Volcanology*, **64**, 316–327.

TEIXELL, A., AYARZA, P., ZEYEN, H., FERNANDEZ, M. & ARBOLEYA, M. L. 2005. Effects of mantle upwelling in a compressional setting: the Atlas Mountains of Morocco. *Terra Nova*, **17**, 456–461.

WOODLAND, A. B. & JUGO, P. J. 2007. A complex magmatic system beneath the Devès volcanic field, Massif Central, France: evidence from clinopyroxene megacrysts. *Contributions to Mineralogy and Petrology*, **153**, 719–731.

ZIEG, M. J. & MARSH, B. D. 2002. Crystal size distributions and scaling laws in the quantification of igneous textures. *Journal of Petrology*, **43**, 85–101.